Numerical Methods in Civil Engineering, 8-1 (2023) 45-57

Numerical Methods in Civil Engineering

Journal Homepage: https://nmce.kntu.ac.ir/

Study of the Elastic and Inelastic Resistance to Lateral Torsional Buckling of Steel Semi-Compact I-Sections

Baker Wael Abuteir * and Abderrahim Labed **

ARTICLE INFO

RESEARCH PAPER

Article history:
Received:
February 2023.
Revised:
July 2023.
Accepted:
July 2023.

Keywords:
Lateral torsional buckling LTB, Local Buckling LB, elastic and inelastic buckling analysis, I-beams, finite element method (FEM) modeling, elastic critical moment Mcr.

Abstract:

This paper uses a parametric numerical study to assess the Lateral-torsional buckling (LTB) performance of several semi-compact beams: S1, S2, and S3. The carrying capacity of these beams, predominantly loaded in bending, is approached by elastic and inelastic buckling analyses. A series of parameters that are believed to influence the resistance to LTB of class 3 beams to (EC3) steel I-beams, namely boundary conditions, flange thickness, and load application level, are investigated. An eigenvalue analysis that predicts the theoretical buckling strength through 3D computational elastic beam models is first conducted using LTBEAM software and ABAQUS. A good agreement in the prediction of M_{cr} was found. Then, a parametric inelastic buckling analysis is performed using the Riks method implanted in ABAQUS. Results have shown the importance of the lateral restraint conditions and the transverse stiffeners to LTB resistance of compressive flange slenderness following EC3-1-1 for cross sections with a class 3 web and class 1 or 2 flange. In addition, an interaction of local buckling (LB) and LTB in the flanges was observed exclusively for restrained beams. The applied load level strongly affects the beams' elastic and inelastic resistance to LTB.

1. Introduction and literature review

Steel members with thin-walled cross-sections are commonly used for long-span beams of industrial halls composite bridges due to their lightness and long-span capacity. The design of steel I-girder sections mainly assumes that flanges provide bending resistance and that the web has a relatively small thickness. The semi-compact sections are susceptible to various forms of instability phenomena. The local buckling reduces the load-carrying capacity of steel members, and their full plastic capacity cannot be reached. Under transverse loads, beams are bent about the major axis and may fail by buckling. One of the primary forms of general stability loss of beams in bending is the Lateral Torsional Buckling (*LTB*).

Physically, the phenomenon of Lateral Torsional Buckling (*LTB*), as depicted in Figure 1, is manifested by changes from initially in-plane bending to combine a large lateral displacement and twist angle and may lead to a partial failure or whole failure in the structure. The complex nature of the *LTB* phenomenon makes it difficult to embrace all the factors and assumptions responsible for it. The factors believed to influence the resistance to *LTB* are namely the distance between lateral or torsional braces, the type, and position of the applied loads, the boundary conditions at the ends and intermediate positions along the beam axis, the material properties, the magnitude and distribution of residual stresses, the initial imperfections and interaction between local and overall buckling. Therefore, lateral torsional buckling should be considered during the design process, as it can significantly reduce load-bearing capacity and affect the safety of the entire structure. Currently, in steel codes (i.e., Eurocode3 and AISC), *LTB* is accounted for in a simplified way by

* *Corresponding author: Ph.D., Faculty of Science and Technology, Civil Engineering Department, University of Tebessa, BP 02, route de Constantine, Tébessa 12000, Algeria. E-mail address: bakerwael.abuteir@univ-tebessa.dz*
** *Senior lecturer in steel structures, Faculty of Science and Technology, Civil Engineering Department, University of Tebessa, BP 02, route de Constantine, Tébessa 12000, Algeria.*

https://doi.org/10.52547/NMCE.2023.760

determining M_{cr}, the critical moment of lateral torsional buckling. The classical case solutions of a cantilever beam carrying a concentrated load at its free edge and the case of a simply supported beam under uniformly distributed moment may be found in traditionally known books [1-3]. However, the literature does not provide analytical solutions for other support conditions.

With the advent of high-performance computer-aided numerical techniques (*FEA*), new solutions to complex lateral-torsional buckling problems have been introduced. Moreover, *LTB* has gained interest in recent years, and many analysis approaches are suggested to assess the lateral torsional buckling behavior of steel members [4,5]. Different material and section properties are also reflected in the studies for identifying the structural behavior in detail [6,7]. Also, the effects of lateral restraints on lateral torsional buckling were investigated for elastic and inelastic regions [8,9]. The literature on different issues related to lateral torsional buckling (*LTB*) of beams is vast, yet in a majority of cases, it focuses on the determination of critical moments with the assumption of fork support as it is in Eurocode3 (*EC3*) [10]. For such idealized support conditions, among others, the impact of some parameters was investigated, such as the distribution of the bending moment [11-14]. Numerous numerical and experimental studies have been performed to predict the ultimate load-carrying capacity of I-beams subjected to lateral torsional buckling. Unterweger et al. [15] investigated beam columns' lateral torsional buckling behavior with one-sided rotation and warping restraints by numerical finite element method (*FEM*) analysis. The ultimate capacity was compared with two different beam-column design methods, the interaction concept (EC3: EN 1993-1-1, 6.3.3) and the general method (EC3: EN 1993-1-1, 6.3.4). An improved *LTB* design curve (buckling reduction factor) was presented. Özbaşaran [16] analyzed the elastic lateral torsional buckling moment of the cantilever I section by finite difference method. Samanta and Kumar [17] studied single symmetric I-sections in which the top and bottom flanges are laterally restrained under different loading cases. The effect of hole diameter and location of lateral torsional buckling strength of composite cantilever beams by experimental and analytical methods were carried out [18]. Balázs and Melcher [19] determined the critical load of steel thin-walled beams with lateral continuous restraint, which is crucial for lateral torsional buckling assessment. An extensive numerical study on lateral torsional buckling of class 4 welded I-section beams at elevated temperatures was performed by [20]. ˇSorf and Jandera [21] studied the lateral torsional buckling behavior by experimental and numerical analysis of welded stainless steel slender I-section beams.

The geometric and material nonlinear properties with imperfection effects were also considered during the analyses. Kuś and Maleska [22,23] proposed a procedure using the Rayleigh-Ritz method to calculate a web-tapered I-beam's critical buckling moment with stiffener ribs. Investigation on lateral torsional buckling of simply supported non-prismatic I-beams with axially varying materials properties according to the volume fraction of the constituent materials based on an exponential or a power law function by a novel finite element formulation and tapered thin-walled beams with singly-symmetric cross-section with arbitrary boundary conditions using finite difference method can be found by Soltani et al. [24,25]. In very recent work, Piotrowski and Szychowski [26] analyzed in a beam the effect of the elastic restraint against warping and rotation in the bending plane compared to classical boundary conditions of fork support communally used and proposed new formulas for several loading cases. The present work investigates some parameters influencing the LTB of semi-compact steel sections. An emphasis on the slenderness of the compressive flange in preventing *LTB* with the interaction with local buckling for a laterally restrained beam.

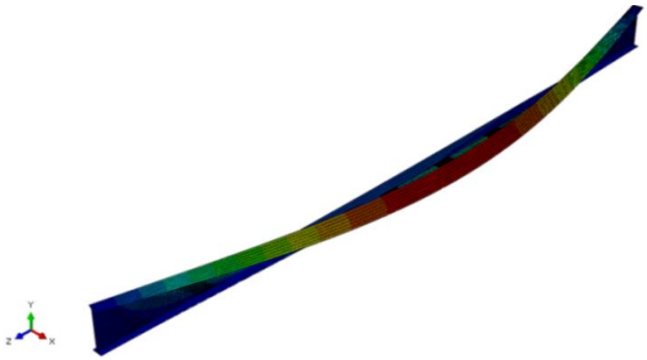

Fig. 1: Lateral torsional buckling phenomenon in a simply supported beam

2. Critical moment to EC3

According to EN 1993-1-1:2005 [10], the beams loaded in the plane of the web and subject to major axis bending should be verified against lateral torsional buckling as follows:

$$M_{Ed} \leq M_{b,Rd} \tag{1}$$

Where M_{Ed} is the design value of the moment and $M_{b,Rd}$ is the design buckling resistance moment defined as:

$$M_{b,Rd} = \chi_{LT} \cdot w_y \cdot \frac{f_y}{\gamma_{M1}} \tag{2}$$

Where w_y is $W_{el,y}$ the appropriate section modulus for class 3 cross-sections, γ_{M1} is the partial factor for buckling

resistance and a recommended value of 1, f_y is the yield strength of the material, and χ_{LT} is the reduction factor for lateral-torsional buckling that ranges from zero to one. For bending members of constant cross-section, the value of χ_{LT} for the appropriate non-dimensional slenderness $\bar{\lambda}_{LT}$ should be determined from the given formulation:

$$\chi_{LT} = \frac{1}{\Phi_{LT} + \sqrt{\Phi^2_{LT} - \bar{\lambda}^2_{LT}}} \quad , \quad \bar{\lambda}_{LT} \le 1 \tag{3}$$

Where, $\Phi_{LT} = 0.5\left(1 + \alpha_{LT}\left(\bar{\lambda}_{LT} - 0.2\right) + \bar{\lambda}^2_{LT}\right)$ and ranges from 0 to 1, α_{LT} is an imperfection factor equal to 0.21 (buckling curve 'a') or 0.34 (buckling curve 'b') and 0.49 (buckling curve 'c') or 0.76 (buckling curve 'd') for rolled and welded sections, respectively, and $\bar{\lambda}_{LT}$ is the non-dimensional slenderness, it is calculated as:

$$\bar{\lambda}_{LT} = \sqrt{\frac{w_y \cdot f_y}{M_{cr}}} \tag{4}$$

Where M_{cr} is the elastic critical Lateral torsional buckling moment and can be analytically evaluated by the 3-factor formula Eurocode3 (*EC3*) for laterally unrestrained beams [27]. It is expressed as follows:

$$M_{cr} = N * \left[\sqrt{\left(\frac{K_z}{K_w}\right)^2 \frac{I_{wi}}{I_{zi}} + \frac{\left(K_z \cdot L\right)^2 GI_{ti}}{\pi^2 EI_{zi}} + \left(C_2 Z_g - C_3 Z_j\right)^2} - \left(C_2 Z_g - C_3 Z_j\right) \right] \tag{5}$$

$$N = C_1 \cdot \frac{\pi^2 EI_{zi}}{\left(K_z \cdot L\right)^2}$$

Where, C_1, C_2, C_3 are factors depending on the loading, end restraint conditions and mono-symmetry of the beam, K_w and K_z are effective length factors which refer to end-warping and to end rotation in plan, respectively, E modulus of elasticity, G shear modulus, L is the length of the beam between points which have lateral restraints, I_t the torsion constant, I_w the warping constant, I_z the second moment of area about the minor axis, z_g is the coordinate of the point of load application, z_j is mono-symmetry parameter.

3. Analysis types

Two types of analysis are conducted to evaluate the ultimate load-carrying capacity of beams subjected to LTB subjected to bending loads, namely the linear and nonlinear buckling analyses.

3.1 Brief theoretical background of linear buckling analysis

The second analysis method used to analyze LTB is through an eigenvalue or Euler buckling analysis, which predicts the theoretical buckling strength of an elastic single beam member. When buckling occurs, eigenvalues are used to describe the values of loads. Then, eigenvectors are used to determine the shape of the calculated eigenvalues. The numerical elastic linear buckling analysis is performed using two software: LTBEAM CTICM [28,29] and ABAQUS [30]. During the linear buckling analysis (*LBA*), the bifurcation point is determined by solving an eigenvalue problem. The eigenvalue problem is solved when the stiffness matrix of the model becomes singular and provides nontrivial solutions. The generalized eigenvalue problem can be carried out as:

$$\left(K + \alpha_{cr} \cdot K_\sigma\right) q = 0 \tag{6}$$

Where α_{cr} is the critical load factor, and q is the mode shape vector. The linear stiffness matrix [31] is defined as follows:

$$K = \int_{V_e} [B]^T D[B] dV \tag{7}$$

Where, B is obtained from a shape function by appropriate differentiation considering the first-order terms of the Green-Lagrange strain and D represents the mechanical properties. The geometric stiffness matrix [32] is also calculated from the following equation:

$$K_\sigma = \int_{V_e} [G]^T S[G] dV \tag{8}$$

Where, G is obtained from a shape function by appropriate differentiation taking into account second-order terms of the Green-Lagrange strain and S is the matrix that represents the state of stress. The main purpose of eigenvalue buckling analysis was to achieve a suitable pattern of imperfection, which is then incorporated into the nonlinear analysis using ABAQUS software.

3.2 Nonlinear post-buckling analysis

The nonlinear analysis solution is accomplished using the RIKS method [30]. This approach is based on the Arc-length method implanted in ABAQUS and is a form of the Newton-Raphson iteration method. Geometric imperfections are also accounted for in the analysis by introducing suitable imperfections shape extracted from the previous *LBA* first mode shape and considered an initial imperfection added to suitable amplitude for the geometric imperfections of ***L/1000*** [33].

4. Local buckling

The local buckling of cross-sections affects their resistance and rotation capacity and must be considered in the design. Local buckling prevents slender or semi-compact sections from attaining full capacity and greatly diminishes their load-bearing capability. This phenomenon is independent of the length of the member and hence is termed local buckling. Also, local buckling involves distortion of the cross-section and treats the safety and serviceability of steel structures. In I-shaped girder steel beams, flanges are parts of plate elements and are relatively thin, and they may undergo local buckling when subjected to compressive forces.

5. Studied cases

The design procedure of beams predominantly loaded in bending is accomplished by considering three cross sections designated as *S1*, *S2*, and *S3*. Sections are bi-symmetric I-shaped sections designed using different flange thicknesses, as shown in Figure 2 and Table 1, made of elastic material (*E=210 GPa*, *v=0.3*) and single span length *L=20 m*. The beams are simply supported and subjected to a uniform distributed load along the beam, with different load positions in the cross-section level. Besides, the effect of variation of lateral boundary conditions at mid-span. According to *EC3* classification criteria, it has been found that for all analyzed sections, the web section is classified in Class 3, while flange sections are of Class 1, 2, or 3, depending on the aspect ratio. Therefore, according to the *EC3* classification criterion, all sections *S1*, *S2*, and *S3* are hence of class 3, being semi-compact.

The dimension of the cross sections is defined as follow:

$$h_w = 1300\ mm\ ,\ b = 300\ mm\ ,\ t_w = 13\ mm$$
$$t_{f1} = 30\ mm\ ,\ t_{f2} = 20\ mm\ ,\ t_{f3} = 15\ mm \quad (9)$$

Table 1: Cross-section geometrical properties of S1, S2 and S3

Geometrical properties	Symbols	Flange thicknesses (*mm*)		
		t_{f1} = 30	t_{f2} = 20	t_{f3} = 15
Cross-sectional area (cm^2)	A	349	289	259
Second moment of area about y (cm^4)	I_y	1034148.3	760768.3	627100.8
Second moment of area about z (cm^4)	I_z	13523.8	9023.8	6773.8
Section modulus about the y-axis (cm^3)	W_{ely}	15208.06	11354.7	9430.08
Torsion constant (cm^4)	I_t	635.2	255.2	162.7
Warping constant (cm^6)	I_w	59805628	39307676	29283564
Static moment (cm^3)	S_y	8731.2	6706.2	5705
Elastic moment (*KN.m*)	M_{ely}	3573.8	2668.3	2216.07
Shear modulus (*Mpa*)	G		80769.2	

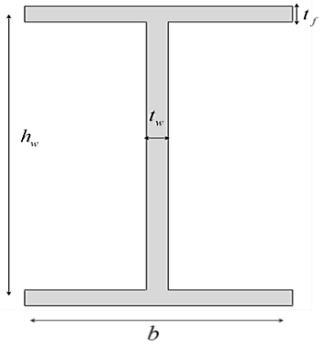

Fig. 2: Typical bi-symmetric steel I-shaped cross-section

Cross section: The cross-sectional geometric dimensions of the finite element model in ABAQUS are depicted in Figure 3. The *X* and *Y* axes define the cross-section plane, and the *Z*-axis defines the longitudinal beam axis. Due to the simplicity of the geometry of I-section beams, an 8-node doubly curved shell element *S8R* has been chosen to model the web and flanges of I-sections.

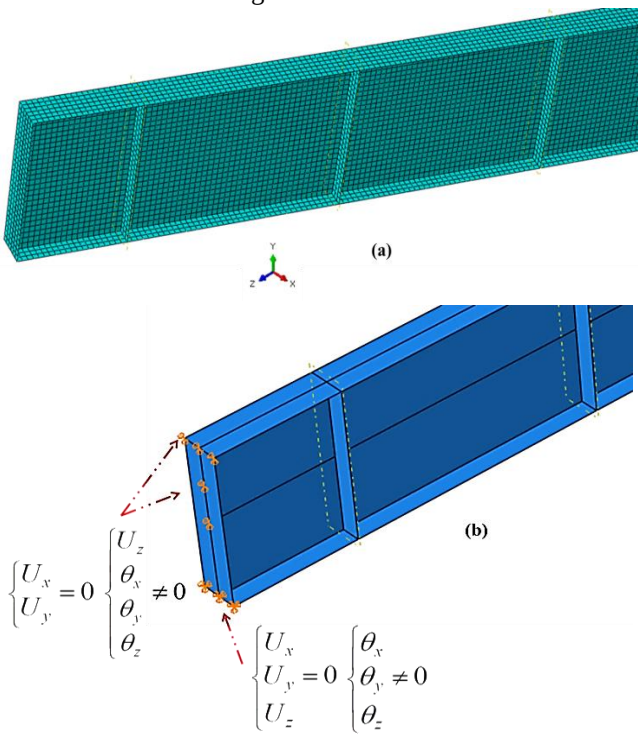

Fig. 3: Typical I-shaped section model implanted in ABAQUS with**(a)** Finite element model of the beam and **(b)** Boundary conditions

Material properties: The material properties of steel grade *S235* are used throughout this investigation. An elastic-plastic stress-strain diagram without strain hardening for the entire model is used, as represented in Figure 4.

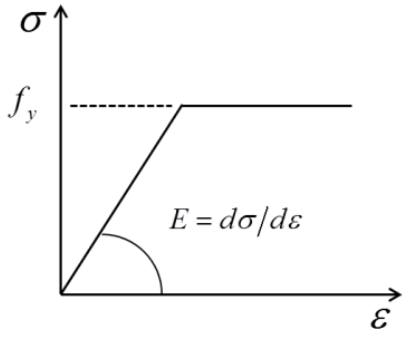

Fig. 4: Bi-linear stress-strain diagram material modeling

Boundary conditions: The used software allows the adoption of common boundary conditions, that is, fork-support as shown in Figure 3(b) or complete fixity. The lateral restraints are modeled for restrained beams by applying a boundary condition at the node that cannot deflect laterally.

Level of the load application: The beams are subjected to transverse uniformly distributed loads at different levels, at the shear center, the top flange, and the lower flange, respectively.

6. Results and discussion

Convergence: Mesh convergence tests have been verified to determine how many elements are required to ensure the efficacy and validation of the presented finite element model.

6.1 Linear buckling analysis

The assessment of the buckling resistance of beams requires the computation of the elastic critical moment, which strongly depends on both the bending moment diagram and end support limitations. A linear buckling analysis (*LBA*) is performed to determine the beam's elastic critical lateral torsional buckling moment. The eigenvalue analysis was conducted assuming small displacements, elastic material behavior, and no imperfections. This numerical study compares the primary extracted results of linear finite element (FE) LTBEAM and ABAQUS with the Eurocode3 (*EC3*) code's formula. These results are used for two purposes: First, to compare the buckling moment results to the analytical solutions Eurocode3 (*EC3*) and finite element (*FE*) results, which can be used later on to validate the computational model and then, the definition of the initial imperfections, based on the first buckling mode shape when executing the inelastic static RIKS analysis 3D models implanted in ABAQUS. Table 2 summarizes the obtained results for all models and shows the obtained values of M_{cr} from the Eurocode3 (*EC3*) formula, LTBEAM, and ABAQUS calculated based on the first *LTB* first mode eigenvalue extracted from software. As it can be noticed, the displaced values of the critical buckling moment are strongly dependent on the flange thickness. M_{cr} values are higher for *S1* (Class 1 flange) than cases with the lowest values for case *S3* (Class 3 flange). This matter can be explained by the smaller slenderness ratio of the compressive flange for the two latter cases

Table 2: Extracted values for the elastic buckling moment

		Unrestrained beams M_{cr} (*KN.m*)			Restrained beams M_{cr} (*KN.m*)		Stiffener members M_{cr} (*KN.m*)
Sections	**Load position**	**Eurocode3 (EC3)**	**LTBEAM**	**ABAQUS**	**LTBEAM**	**ABAQUS**	**ABAQUS**
S1	**Top**	643.074	638.03	641.855	2624.8	2588.3	664.807
	Shear centre	850.133	846.11	863.755	2946.9	2827.825	897.039
	Bottom	1123.254	1127.2	1181.466	3305.7	3042.325	1218.503
S2	**Top**	356.806	356.78	366.209	1636.5	1664.832	382.591
	Shear centre	489.857	493.11	507.933	1848.1	1827.58	530.638
	Bottom	672.061	680.96	720.893	2085.2	1971.652	746.959
S3	**Top**	254.356	255.41	264.324	1206.3	1245.392	279.016
	Shear centre	352.919	356.43	370.116	1364	1371.704	389.594
	Bottom	489.433	496.99	530.244	1540.9	1482.504	552.005

Table 3: Comparison of LTBEAM and ABAQUS critical moments predictions for unrestrained beams

Sections		**S1**			**S2**			**S3**		
Load position		**Top**	**Shear centre**	**Bottom**	**Top**	**Shear centre**	**Bottom**	**Top**	**Shear centre**	**Bottom**
Unrestrained (LTBEAM)	α_{cr}	0.17361	0.2367	0.3153	0.1334	0.1843	0.2546	0.1148	0.1602	0.2234
	M_{cr} (***KN.m***)	638.03	846.11	1127.2	356.78	493.11	680.96	255.41	356.43	496.99
Unrestrained (ABAQUS)	α_{cr}	0.17954	0.24161	0.33048	0.13726	0.19038	0.27020	0.11928	0.16702	0.23928
	M_{cr} (***KN.m***)	641.855	863.755	1181.466	366.209	507.933	720.893	264.324	370.116	530.244
Difference (%)		0.599	2.085	4.814	2.642	3.006	5.864	3.490	3.839	6.691

Table 4: Comparison of LTBEAM and ABAQUS critical moments predictions for restrained beams

Sections		**S1**			**S2**			**S3**		
Load position		**Top**	**Shear centre**	**Bottom**	**Top**	**Shear centre**	**Bottom**	**Top**	**Shear centre**	**Bottom**
Restrained (LTBEAM)	α_{cr}	0.734	0.824	0.924	0.611	0.690	0.779	0.5422	0.613	0.692
	M_{cr} (***KN.m***)	2624.8	2946.9	3305.7	1636.5	1848.1	2085.2	1206.3	1364	1540.9
Restrained (ABAQUS)	α_{cr}	0.724	0.791	0.851	0.624	0.685	0.739	0.562	0.619	0.669
	M_{cr} (***KN.m***)	2588.3	2827.825	3042.325	1664.832	1827.58	1971.652	1245.392	1371.704	1482.504
Difference (%)		1.410	4.210	8.657	1.701	1.122	5.759	3.138	0.564	3.939

Results show that the ABAQUS outcomes regarding M_{cr} are very close to those from LTBEAM. This comparison provides additional confidence to the ABAQUS model when it is used later on for the inelastic analysis, as it can be seen in Figure 5, which depicts graphically the variation of the values of M_{cr} in terms of flange's thickness or flange's slenderness, that a significant decrease when the flange thickness increases. Also, the position of the applied load in the section is critical as it shows larger values for M_{cr} when located on the compressive flange and minor values at the shear center and tension flange, respectively. The use of analytical Equatin (5) of *EC3* leads to very close values of M_{cr} to results of LTBEAM and ABAQUS with slight differences both for unrestrained and restrained beams.

The differences in values of M_{cr} are minimal and range from 0.6 to 8% depending on the variation of boundary conditions and load positions.

Tables 3 and 4 demonstrate the differences (%) for unrestrained and restrained beams from LTBEAM and ABAQUS outcomes, respectively, regarding load positions. Furthermore, numerical linear buckling eigenvalues results have shown that the obtained values of M_{cr} have shown a good correlation between LTBEAM and ABAQUS. That is ABAQUS results that are, on average, 1.3% larger than the results of LTBEAM, with a standard deviation of 0.02. M_{cr} values at the bottom position are higher than the others. The reason is mainly because the bottom is in the tension zone, free from buckling. Figure 6 depicts the first mode shapes of the lateral torsional buckling for unrestrained, restrained beams equipped with two symmetrical transverse stiffeners. In Table 5, the design resistance buckling moment values are indicated.

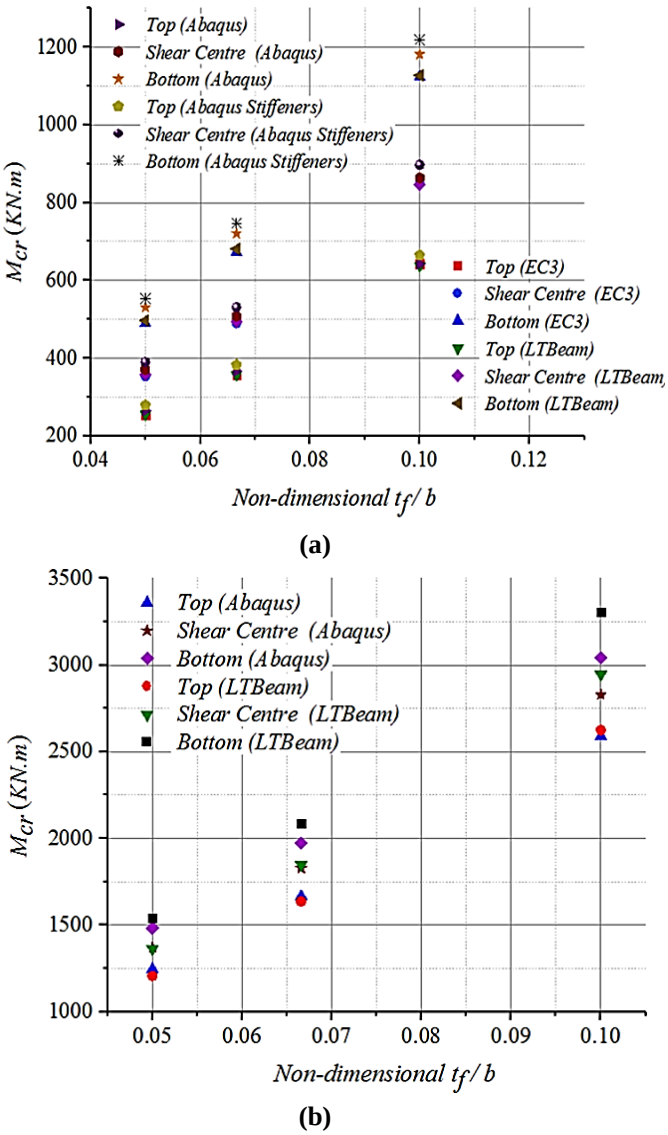

Fig. 5: Elastic critical variation of critical LTB moment: **(a)** Unrestrained beam **(b)** Lateral restraint beam

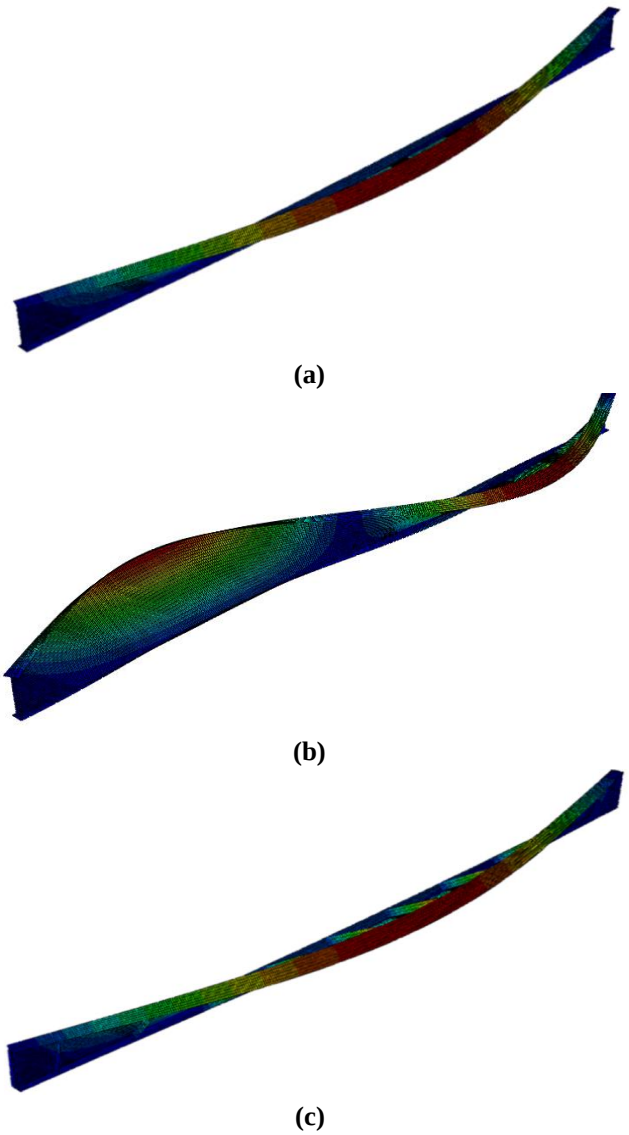

Fig. 6: Lateral torsional buckling deformed shape of the first mode for **(a)** unrestrained, **(b)** restrained, and **(c)** beam with transverse stiffeners.

Table 5: Design buckling resistance moment

Sections	Load position	$\bar{\lambda}_{LT} \geq 0.4$	α_{LT}	Φ_{LT}	$\chi_{LT} \leq 1$	$M_{b,Rdi}$ **(*KN.m*)**	$M_u = M_{el,yi}$ **(*KN.m*)**
S1	**Top**	2.357	0.76	4.097	0.134	478.901	3573.894
	Shear centre	2.050		3.304	0.17	607.562	
	Bottom	1.783		2.691	0.212	757.665	
S2	**Top**	2.734		5.200	0.103	274.841	2668.366
	Shear centre	2.334		4.034	0.136	362.897	
	Bottom	1.992		3.164	0.177	472.300	
S3	**Top**	2.951		5.899	0.090	199.446	2216.070
	Shear centre	2.505		4.513	0.120	265.928	
	Bottom	2.127		3.494	0.159	352.355	

6.2 Inelastic buckling analysis results

The discussion is based on the derived load-deflection curves from the modified RIKS analysis implanted in ABAQUS. Hence, for every single step, the displacement and stiffness matrices are updated, including initial geometrical imperfection, which is liable to trigger off torsion or lateral bending, is obviously of concern, and typically, with residual stresses (not considered in this study).

6.2.1 Unrestrained beam

First of all, it should be noted that both load and boundary conditions have very significant effects on the inelastic LTB failure mode results. The results from the modified RIKS method are given in terms of load proportionality factor λ (*LPF*). The applied load on the model must be multiplied by the *LPF* to determine the actual critical load, indicating the point right before instability occurs. Table 6 gives the load proportionality factor (*LPF*) and the actual critical load of the unrestrained beam.

Table 6: LPF and actual failure load

Sections	Load positions	Load (*P*) (*KN*)	LPF	Actual failure load (*KN*)
S1	Top	25.597	1.07	27.388
	Shear Centre	34.463	1	34.463
	Bottom	47.19	0.96	45.302
S2	Top	14.659	1.16	17.004
	Shear Centre	20.33	1.06	21.549
	Bottom	28.89	0.99	28.601
S3	Top	10.591	1.21	12.815
	Shear Centre	14.863	1.09	16.200
	Bottom	21.271	1	21.271

Generally speaking, the slope of the load-deflection curve represents an equivalent (generalized) stiffness to express the resistance to *LTB*. In common practice, the point corresponding to zero slopes is the critical load and the maximum associated moment in the vertical plane. This moment is regarded as the critical moment, which is very close to flange buckling by bending about the weak axis of the cross-section.

Figure 7 represents the outcomes of the unrestrained beams, while Figure 9 is intended to give the results of restrained beams during the whole loading history by considering three load positions. Figures 7 and 9 show that the beams behave nonlinearly due to the initial geometric imperfections and the nonlinear geometry conditions.

As far as unrestrained beams are concerned, Figure 7 depicts the load-lateral deflection curves. As can be seen, two distinct branches are characterized by linear pre-critical behavior for the first branch, and an inelastic post-buckling behavior is recognized in the second branch, namely the decrease in stiffness. The load-lateral deflection curve starts to soften, which means that the capability to resist *LTB* starts to degrade. The observed tendency of all studied I-beams subject to *LTB* to twist about their longitudinal axis, and it is suspected that such I-beams contain a form of negative rotational stiffness about their longitudinal axis.

It is evident from Figure 7 that linear load-deflection behavior exists before inelastic lateral buckling starts to occur. It can be deduced from Figure 7 that when a buckling instability occurs, the beam contains a form of negative stiffness. It is evident that varying flange slenderness, the member capacity, is governed by the inelastic capacity, as mentioned in the previous section. In the cases of unrestrained beams, a soft decrease in stiffness in the post-buckling behavior can be observed.

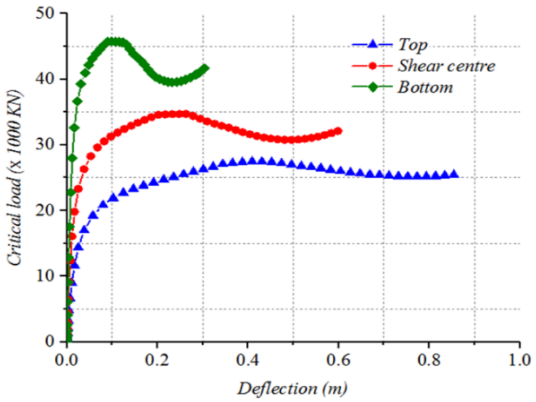

(a)

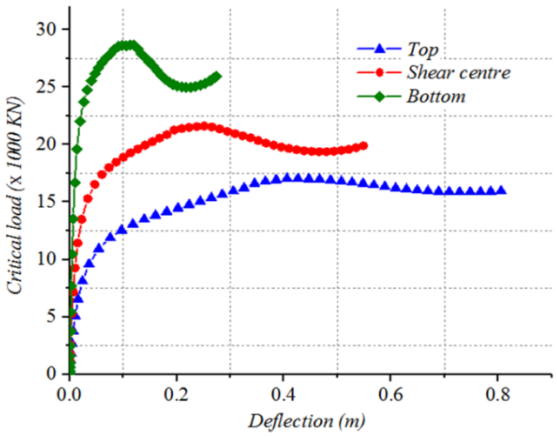

(b)

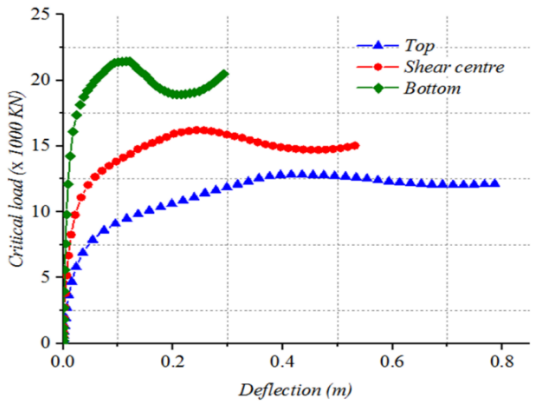

(c)

Fig. 7: Critical load versus lateral deflection of unrestrained beam for **(a)** sections S1, **(b)** S2, and **(c)** S3, respectively.

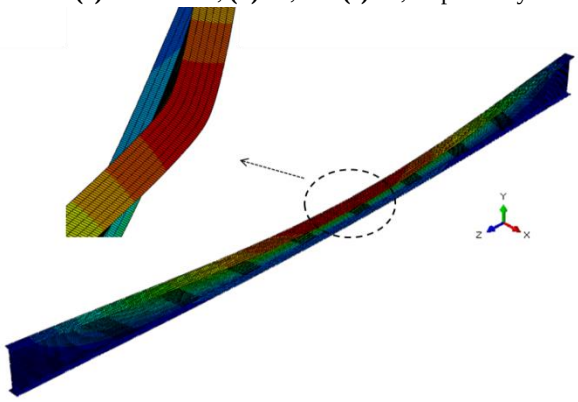

Fig. 8: Lateral torsional buckling for the unrestrained beam at the ultimate increment

Figure 8 shows the deformed shape of the unrestrained beam at the ultimate increment with load applied at the top flange of *S1*. It produces a large lateral displacement due to the beam's high bending stiffness without considering the effect of stiffeners on the behavior of the whole I-beam.

6.2.2 Restrained beam

The same arguments discussed in the above section apply to laterally restrained beams. However, the critical buckling load in the post-buckling characteristic of the sudden phenomenon has a slight slope after the buckling point. The lateral restraint is located in the middle of the top flange of the beam. This measure prevents the beam from deflecting laterally and increases consequently M_{cr}. Figure 9 shows that the thicker flange leads naturally to a more significant value of P_{cr}. This matter is evident from the slope of the curve after the critical load is reached, and a beam was observed to have deformed significantly while the current load decreased. Figure 10 shows the deformed shape of the restrained beam at the ultimate stage with load applied at the top flange of *S1*. Table 7 gives the load proportionality factor (*LPF*) and the actual critical load of the restrained beam.

Table 7: LPF and actual failure load

Sections	Load positions	Load (*P*) (*KN*)	LPF	Actual failure load (*KN*)
S1	**Top**	103.532	0.96	99.390
	Shear Centre	113.113	0.86	97.277
	Bottom	121.693	1.64	199.576
S2	**Top**	66.768	0.94	62.761
	Shear Centre	73.295	0.85	62.300
	Bottom	79.073	1.65	130.470
S3	**Top**	50.018	0.98	49.017
	Shear Centre	55.091	0.98	53.989
	Bottom	59.541	1.71	101.815

Once again, as it was for unrestrained beams, Figure 9 gives two distinct behaviors, pre- and post-bucking, in terms of load vs. lateral deflections. For laterally restrained beams, even with higher values of critical loads, the loss of stiffness is remarkable, with a more pronounced tendency with slight variation in the lateral displacements. The buckling capacity of LTB significantly increases when using a kind of lateral restraint, unlike the unrestrained beam. However, when the critical load is reached, a severe decrease in stiffness of all beams, especially for *S1* compared to *S2* and *S3* similar decreases have been noticed with less brutality. Indeed, when the beam approaches its collapse state, it becomes increasingly flexible in its stiffness. According to the results of the present study, and surprisingly enough, while expecting the failure of beams as the lateral deflection becomes more significant with a severe drop of the stiffness, a positive stiffness appears in all studied cases with different amounts, particularly when the load is applied in the tension flange. To the authors' knowledge, that is the first time it has been reported, expressing the particular effect of the lateral restraint parameter, which plays an essential role in the post-buckling behavior of semi-compact class 3 I-beams shaped. However, as previously mentioned, this tendency is less critical when dealing with unrestrained beams. It is probably because the beam is stable, stemming from the intermolecular structures getting closer to each other and automatically gaining certain rigidity as the displacement decreases, leading to a positive stiffness to the beam. Figure 11 illustrates the deformed shape of the beam with stiffener members at ultimate increment with load applied at the top flange of *S1*, respectively.

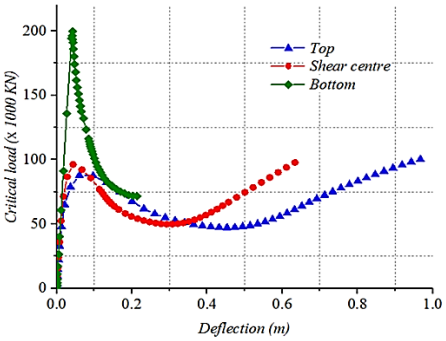

(a)

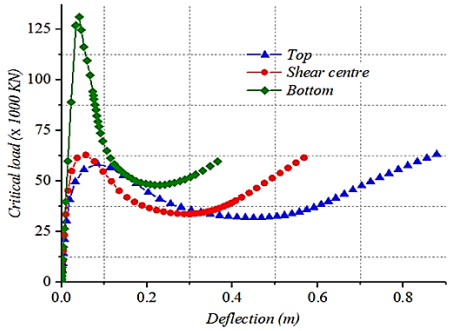

(b)

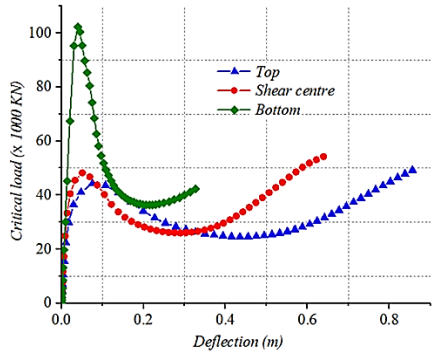

(c)

Fig. 9: Critical load versus lateral deflection of restrained beam for **(a)** sections S1, **(b)** S2, and **(c)** S3, respectively

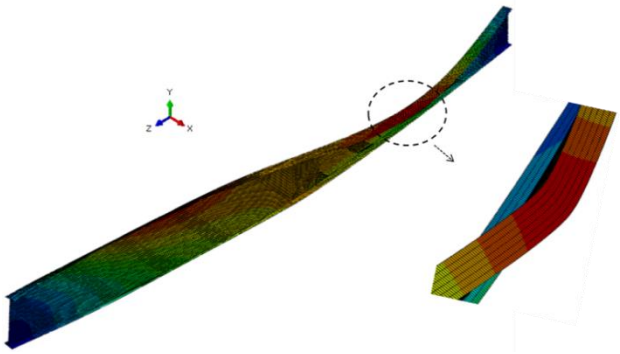

Fig. 10: Lateral torsional buckling for the restrained beam at the ultimate increment

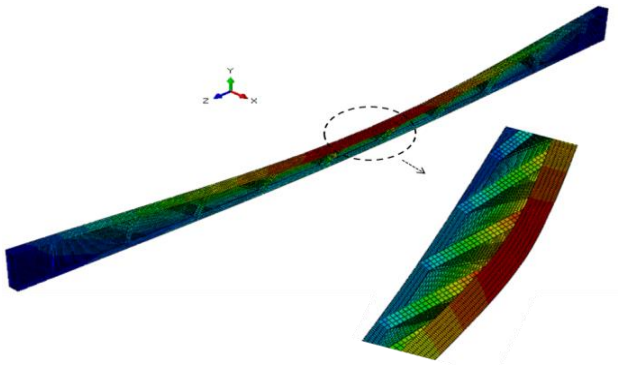

(a)

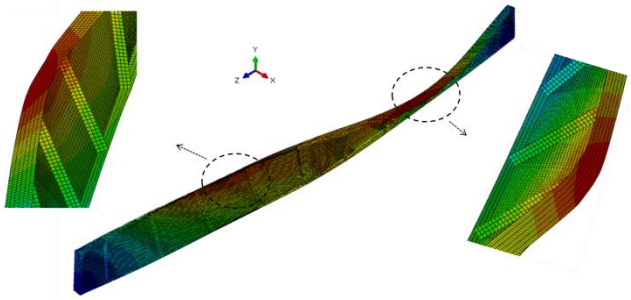

(b)

Fig. 11: Lateral torsional buckling for **(a)** beam with stiffeners; **(b)** restraint and stiffeners together

6.3 Local buckling observations

First, it is worth recalling that study case 3, i.e., *S3*, with lateral restraint, was composed of symmetrical flanges of class 3 along with the web. The lateral restraint was considered to avoid lateral torsional buckling. Figures 12-15 depict that for *S3* exclusively having flange Class 3, the local buckling instability phenomenon at the ultimate loading increment results in local deformation of flanges of I beam: upper and lower flanges, respectively. It can also be said that an interaction of LTB with local buckling in the upper flange phenomena has occurred. As seen in Figure 12-14, the general shape of the deformation looks like a continuous thin plate in flexion, which indicates that flanges are suffering from local buckling. The obtained results are in concordance with *EC3* clause 6.2.1 for class 3 cross-sections, where the resistance of all the compression parts of a cross-section that is of Class 3 should be based on an elastic distribution of strains across the cross-section. For Class 1 and 2 flanges, the local buckling was not observed, which is following *EC3, which* envisages some exceptions to the general procedure for the classification. For cross sections with a class 3 web and Class 1 or 2, flanges may be classified as class 2 cross sections with an effective web in accordance (clause 5.5.2(11)).

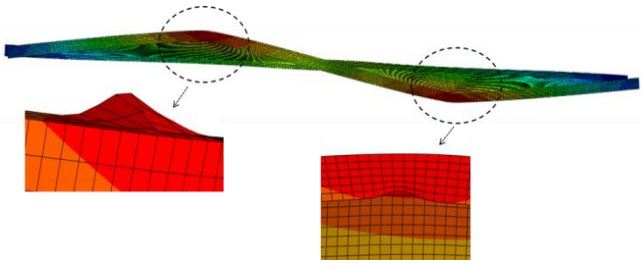

Fig. 12: Local buckling at the upper flange of the stiffened beam at ultimate increment with load applied at the top of the flange and shear center of *S3*, respectively.

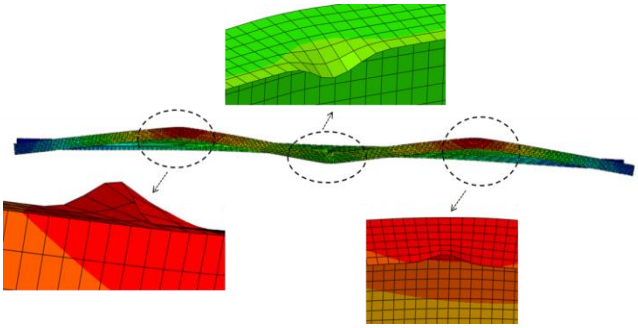

Fig. 13: Local buckling at the upper flange of stiffened beam at ultimate increment with load applied at the bottom of the flange of *S3*.

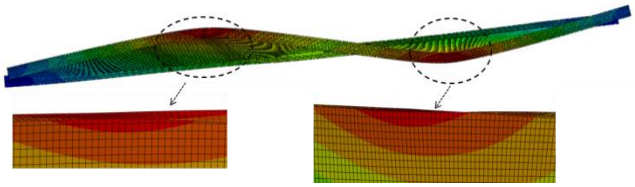

Fig. 14: Lateral torsional buckling without local buckling appearance at the upper flange of the stiffened beam at ultimate increment with different positions of applied load of *S1* and *S2*.

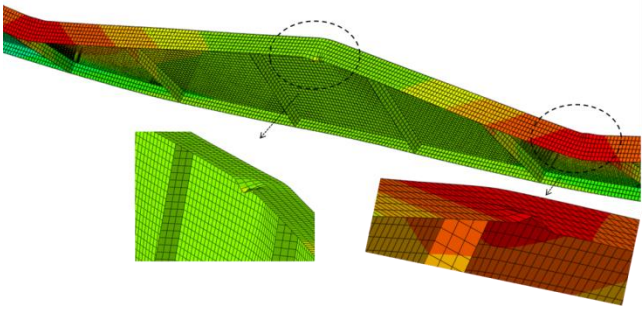

Fig. 15: Local buckling at the upper flange of stiffened with stiffeners members along the beam at ultimate increment with load applied at the bottom of the flange of *S3*.

7. Conclusion

Lateral Torsional Buckling (*LTB*) is a buckling mode involving lateral deflection and twisting in flexure members. This study investigates the potential of bi-symmetrical semi-compact beams subject to *LTB*. Although both elastic and inelastic behaviors of *LTB* are captured in this study, this research has some limitations as the effect of residual stresses is not considered. A series of parameters have been investigated, including member slenderness, degree of lateral restraint, type of loadings, initial imperfections, and stiffener members. Some concluding remarks can be drawn.

- It was found that the studied parameters strongly affect the capacity of a beam to undergo large displacements in the inelastic range.
- The present study's finding confirms the statement made by Uy [34]: when buckling occurs in the inelastic range, the stiffness is reduced, and the post-buckling response is generally affected rather than the ultimate load capacity.
- The results of this study confirm the statement made in *EC3* 6.2.2.4 (clause 5.5.2(11)) about the compressive flange of sections 1 or Curves 9 and 10, highlighting the significant effects of parameters.
  Regarding the effect of flange's class in the global behavior of class 3 sections, results confirm the *EC3* statement in clause 5.5.2, dealing with some exceptions to the general procedure for the classification. When the flange is of Class 1 or 2, compressive dimensions (or slenderness) confirm for cross sections with a Class 3 web, and Class 1 or 2 flanges may be classified as Class 2 cross sections with an effective web in accordance (clause 5.5.2(11)).
- The load position in the cross-section and the lateral conditions can improve the carrying capacity of beams to *LTB*, especially in their inelastic response concerning these parameters. Choosing a compressive flange of class 1 has been found to give better results regarding the *LTB* resistance of the whole section. Although imperfections are considered, higher resistance levels are usually obtained for thicker compressive flange along with the load locations in the cross-section.
- A post-buckling behavior is observed in the restrained beams. For laterally restrained beams under high levels of large deflection, the intermolecular structures of the material get closer to each other and automatically provide a certain additional positive rigidity to the beam, leading to post-elastic beam stability.
- Placing several transverse stiffeners has shown a particularly positive contribution to the carrying capacity of beams to *LTB*. More investigation is needed to confirm such a result.
- Also, in future work, the interaction of *LTB* and the local buckling, being not a limiting criterion, by the more refined meshing of the web section, can be of interest.
  Finally, the natural resistance to LTB of the semi-compact steel section is mainly related to the flange's class section. Better performance of I-shaped steel structures can be observed with flanges class 1 or 2 as they can develop plastic behaviors.

Funding: This research received no specific grant from public, commercial, or not-for-profit funding agencies.

References

[1] Timoshenko, S. P., & Gere, J. M. (1963). *Theory of Elastic Stability*. 2nd ed., New York:: McGraw-Hill.

[2] Chajes, A. (1974). *Principles of Structural Stability*. 1st ed., New Jersey:: Prentice-Hall.

[3] Trahair, N. S. (1993). *Flexural-Torsional Buckling of Structures*. 1st ed., E & FN SPON, London:: Taylor & Francis Group.

[4] Benyamina, A. B., Meftah, S. A., Mohri, F., & Daya, E. M. (2013). Analytical solutions attempt for lateral torsional buckling of doubly symmetric web-tapered I-beams. *Engineering Structures, 56*, 1207-1219.

[5] Ozbasaran, H., Aydin, R., & Dogan, M. (2015). An alternative design procedure for lateral-torsional buckling of cantilever I-beams. *Thin-Walled Structures, 90*, 235-242.

[6] Wang, Y. Q., Yuan, H. X., Shi, Y. J., & Chenk, M. (2012). Lateral-torsional buckling resistance of aluminum I-beam. *Thin-Walled Structures, 50*, 24-36.

[7] Da Silva, L. S., Rebelo, C., Nethercot, D., Marques, L., Simões, R., & Real, PMM. (2009). Statistical evaluation of the lateral–torsional buckling resistance of steel I-beams. Part 2: Variability of steel properties, *Journal of Constructional Steel Research, 65,* 832-849.

[8] Rahair, N. S. (2009). Buckling analysis design of steel frames. *Journal of Constructional Steel Research, 65*, 1459-1463.

[9] Piotrowski, R., & Szychowski, A. (2019). Lateral Torsional Buckling of Steel Beams Elastically Restrained at the Support Nodes. *Applied Sciences, 9*, 1-17.

[10] EN 1993-1-1:2005. (2005). Eurocode 3 Design of steel structures-Part 1-1: General rules and rules for buildings, *European Committee for Standardization (CEN)*, Brussels.

[11] López, A., Yong, D. J., & Serna, M. A. (2006). Lateral-torsional buckling of steel beams: A general expression for the moment gradient factor. *In Proceedings of the Stability and Ductility of Steel Structures Lisbon*, Portugal.

[12] Li, X. X. (2007). Flexural strength for general lateral-torsional buckling. *Journal of Structural Engineering, 133*, 674-682.

[13] Trahair, N. S., Bradford, M. A., Nethercot, D. A., & Gardner, L. (2008). The Behaviour and Design of Steel Structures to EC3. *Taylor and Francis, (4)*, London, New York.

[14] Yilmaz, T., & Kirac, N. (2016). On the Evaluation of Critical Lateral-Torsional Buckling Loads of Monosymmetric Beam-Columns. *World Academy of Science, Engineering, and Technology International Journal of Civil and Environmental Engineering, 10*, 885-892.

[15] Unterweger, H., Taras, A., & Feher, Z. (2016). Lateral-torsional buckling behavior of I-section beam-columns with one-sided rotation and warping restraint. *Steel Construction, 9*, 24-32.

[16] Özbaşaran, H. (2013). Finite differences approach for calculating elastic lateral torsional buckling moment of cantilever I section. *Journal of Science and Technology, 14*, 143-152.

[17] Samanta, A., & Kumar, A. (2008). Distortional buckling in braced-cantilever I-beams. *Thin Walled Structures, 46*, 637-645.

[18] Eryiğit, E., Zor, M., & Arman, Y. (2009). Hole effects on lateral buckling of laminated cantilever beams. *Composites Part B: Engineering, 40*, 174-179.

[19] Balázs, I., & Melcher, J. (2015). Lateral torsional buckling of steel thin-walled beams with lateral restraints. *International Journal of Civil, Engineering, Structural, Construction and Architectural Engineering, 9*, 730-735.

[20] Jandera, M., Prachar, M., & Wald, F. (2020). Lateral torsional buckling of class 4 section uniform and web tapered beams at elevated temperature. *Thin Walled Structures, 146*, 1-12.

[21] ˇSorf, M., & Jandera, M. (2020). Lateral-torsional buckling of slender cross-section stainless steel beams. *Structures, 28*, 1466-1478.

[22] Kuś, J., & Maleska, T. (2021). Lateral torsional buckling of tapered steel I-beams with stiffener ribs. *Modern Trends in Research on Steel, Aluminium and Composite Structures*, 428-434.

[23] Kuś, J. (2015). Lateral–torsional buckling steel beams with simultaneously tapered flanges and web. *Steel Composite Structures An International Journal, 19*(4), 897-916.

[24] Soltani, M., Asgarian, B., & Mohri, F. (2019). Improved Finite Element Model for Lateral Stability Analysis of Axially Functionally Graded Nonprismatic I-beams. *International Journal of Structural Stability and Dynamics, 19*(9), 1-38.

[25] Soltani, M., Asil Gharebaghi, S., & Mohri, F. (2018). Lateral stability analysis of steel tapered thin-walled beams under various boundary conditions. *Numerical Methods in Civil Engineering journal, 3*(1), 13-25.

[26] Piotrowski, R., & Szychowski, A. (2022). The Effect of Steel Beam Elastic Restraint on the Critical Moment of Lateral Torsional Buckling. *Materials, 15*(4), 1275.

[27] Andrade, A., Camotim, D., & Providência, e Costa P. (2007). On the evaluation of elastic critical moments in doubly and singly symmetric I-section cantilevers. *Journal of Constructional Steel Research, 63*, 894-908.

[28] CTICM, LTBeam. (2001). Saint-Aubin, France.

[29] Galéa, Y. (2003). Moment critique de déversement élastique de poutres fléchies présentation du logiciel LTBEAM. *Revue Construction Métallique*, CTICM. https://www.cticm.com/centre-de-ressources.

[30] Dassault Systèmes Simulia Corp, ABAQUS/Standard User's Manual, version 6.13. (2013). Providence, RI. www.simulia.com.

[31] Oñate. (1992). *Cálculo de Estructuras por el Método de Elementos Finitos*. 1st ed., Spain :: CIMNE.

[32] Clark, J. W., & Hill, H. N. (1960). Lateral buckling of beams. *Journal of Structural Division, 86*, 175-196.

[33] Chan, S. L. (2009). *Guide on second-order and advanced analysis of structures*. 2nd version.

[34] UY, B. (2006). Local and interaction buckling of composite construction members. in: Shanmugan, N. E., & Wang, C. M. (2nd Eds.), Analysis and Design of Plated Structures. *Woodhead Publishing Series in Civil and Structural Engineering, School of Civil Engineering*, University of Sydney, NSW, Australia. 343-363. https://doi.org/10.1016/B978-0-12-823570-6.00017-3